Effect of size polydispersity on the crystal-fluid and crystal-glass transition in hard-core repulsive Yukawa systems

Marjolein N. van der Linden, Alfons van Blaaderen, and Marjolein Dijkstra

Citation: J. Chem. Phys. **138**, 114903 (2013); doi: 10.1063/1.4794918
View online: http://dx.doi.org/10.1063/1.4794918
View Table of Contents: http://jcp.aip.org/resource/1/JCPSA6/v138/i11
Published by the American Institute of Physics.

Effect of size polydispersity on the crystal-fluid and crystal-glass transition in hard-core repulsive Yukawa systems

Marjolein N. van der Linden,[a] Alfons van Blaaderen, and Marjolein Dijkstra[b]
Soft Condensed Matter, Debye Institute for Nanomaterials Science, Utrecht University, Princetonplein 5, 3584 CC Utrecht, The Netherlands

(Received 1 August 2012; accepted 14 February 2013; published online 19 March 2013)

We investigated the effect of size polydispersity on the crystal-fluid transition in hard-core repulsive Yukawa systems by means of Monte Carlo simulations for several state points in the Yukawa parameter space. Size polydispersity was introduced in the system only with respect to the hard particle cores; particles with different diameters had the same surface potential ψ_0, but the charge per particle was not varied with packing fraction or distance. We observed a shift to higher packing fraction of the crystal-fluid transition of bulk crystals with a fixed log-normal size distribution upon increasing the polydispersity, which was more pronounced for weakly charged particles ($\psi_0 \approx 23$ mV) compared to more highly charged particles ($\psi_0 \approx 46$ mV), and also more pronounced for larger Debye screening length. At high polydispersities ($\geq$0.13) parts of the more highly charged systems that were initially crystalline became amorphous. The amorphous parts had a higher polydispersity than the crystalline parts, indicating the presence of a terminal polydispersity beyond which the homogeneous crystal phase was no longer stable. © *2013 American Institute of Physics*. [http://dx.doi.org/10.1063/1.4794918]

I. INTRODUCTION

For certain charge-stabilized colloidal systems, such as well-index-matched particles and/or colloids with a thick enough steric stabilization layer, the always-present and attractive Van der Waals forces can be neglected.[1] The interactions between such like-charged colloids can be described by the hard-core repulsive Yukawa (screened Coulomb) potential, an effective pair potential that results after the degrees of freedom of the microions have been integrated out. The equilibrium phase behavior for colloidal spheres interacting through a Hard-Sphere-Yukawa (HSY) potential is well known from computer simulations[2–4] and experiments.[5–10] In the (packing fraction η, Debye screening length $(\kappa\sigma)^{-1}$) plane of the phase diagram, a fluid is found at low packing fractions and two different crystal structures at higher packing fractions: a face-centered-cubic (fcc) crystal at small screening lengths and a body-centered-cubic (bcc) crystal at larger screening lengths and moderate packing fractions, flanked by an fcc crystal at higher packing fractions. The exact locations of the phase boundaries depend on the details of the model system, i.e., the charge on the colloids, the salt concentration, and the dielectric constant of the solvent.

Almost all phase diagrams for the HSY systems were calculated under the assumption that the particles are monodisperse in size, i.e., that all particles have the same diameter, and many for a fixed contact value of the interaction potential.[2–4] In real colloidal dispersions, however, both are never truly the case. In an experimental system the distribution of particle diameters is determined by the synthesis of the particles and can approximately be described by a Gaussian or log-normal distribution.[1] The system can be viewed as containing an effectively infinite number of particle species (each having a different diameter), and we call the system therefore size *poly*disperse.[11] The polydispersity is commonly defined as the ratio of the standard deviation and the mean of the size distribution. In experimental systems the charge on the particles is affected by the local chemical potential of the charge-determining ions; the two limiting cases are described by assuming constant-charge or constant-potential boundary conditions on the particle surface.[12]

For the case of hard spheres (or approximations thereof), phenomena arising from the presence of polydispersity have been investigated theoretically,[13–23] computationally[15,21–25] and experimentally[26–29] (for a review see Ref. 11). We first consider the case of quenched polydispersity, i.e., where the polydispersity in the coexisting phases is kept (nearly) constant and where fractionation is thus not allowed. In experiments it has been observed that above a certain value of the polydispersity, crystallization in the system does not occur.[27] This *terminal polydispersity* is thought to arise because with increasing polydispersity the particles fit less well on the crystal lattice and the crystal structure is destabilized. At sufficiently high polydispersity the free energy of the fluid becomes lower than that of any crystal phase. The terminal polydispersity is the maximal polydispersity that a single stable crystalline phase can have. Several theoretical and computational studies provide estimates for the value of the terminal polydispersity (ranging from ~0.05 to 0.12), see, e.g., Refs. 13–15, and 24. For polydispersities just below the terminal polydispersity *reentrant melting* was found at higher packing fractions in theoretical work[16] and experiments.[28] Others report instead a crystal-to-glass transition, due to the

[a]Electronic mail: M.N.vanderLinden@uu.nl.
[b]Electronic mail: M.Dijkstra1@uu.nl.

presence of an equilibrium glassy phase at high densities and high polydispersities;[19] also experimentally a polydispersity-induced crystal-to-glass transition has been observed.[29] These findings could be explained by noting that with increasing polydispersity, the maximum packing fraction for an ordered 3D crystal decreases, while it increases for a fluid or disordered glassy state,[15,25] making the fluid or glass the thermodynamically stable phase at high packing fractions.[16] For systems interacting through a softer pair potential than the hard-sphere potential, terminal polydispersities have been found as well. Monte Carlo simulations revealed a crystal-to-glass transition in systems of polydisperse charged colloids interacting through a HSY pair potential.[30] In semigrand ensemble simulations a terminal polydispersity was reported for a soft-sphere system, which in the crystalline phase increased with increasing potential softness.[31] In recent simulation work a terminal polydispersity as well as reentrant melting were found for HSY systems with quenched size polydispersity using free energy calculations.[32]

A common feature in the above-mentioned theoretical and computational studies is that the polydispersity in the coexisting phases was kept constant. For the hard-sphere system, simulation work was also carried out under different conditions where the size distribution in the coexisting phases was allowed to vary. This gives rise to the phenomenon where the system splits into two or more coexisting phases with different polydispersities, so-called *fractionation*. One scenario where fractionation occurs is when a fluid with large size polydispersity ($\sim$0.12) coexists with a crystal that has a narrower size distribution ($\sim$0.06).[17] However, the simulations that led to this result were carried out in the semigrand canonical ensemble, which fixes the chemical potential differences for different particle sizes with respect to some reference particle, but not the overall particle size distribution in the system, thus allowing for variable polydispersity. Later, solid-fluid coexistence with fractionation was found in more realistic theory and simulation work for the experimentally relevant situation of a fixed overall size distribution.[18,22] Also, in theoretical and computational studies the coexistence of multiple solid phases was found, each with a narrow size distribution, in a system with a large overall polydispersity and a fixed overall size distribution.[18,21,23] It should be noted here that, when given enough time, a system can of course always divide itself up in less polydisperse subsystems that then may form crystal phases. However, since fractionation requires significant long-distance particle diffusion, it is expected that in experimental systems extensive fractionation will take (inaccessible) long times.[20]

The outcome of experiments on systems with polydisperse particles will thus not only be determined by equilibrium thermodynamics, but also by *non-equilibrium phenomena*. The above-mentioned experimentally observed absence of crystallization above a certain polydispersity value could also be due to slow dynamics (the dynamic glass transition), or high nucleation barriers, which are known to increase with polydispersity.[27,33] Simulation work on a soft-sphere system predicts that while a first-order freezing transition up to a polydispersity of 0.45 is present, in experiments non-equilibrium effects will dominate at polydispersities above 0.12.[34]

Most experimental work on HSY systems has been performed on colloidal systems where the double layer thickness (κ^{-1}) is smaller than the particle diameter (σ). However, recently there has been renewed interest in soft systems where the double layer thickness is on the order of the particle size or larger.[7,35] Inevitably, polydispersity is present in these experimental systems as well, although the nonlinear double-layer interaction is expected to make its effects on phase behavior less strong than for hard-sphere systems. Preliminary experimental observations indicate that the long-range interactions enable the crystal structure to accommodate a very large polydispersity.[36] In this work we move beyond the simple hard-sphere-like colloidal systems and investigate the phenomena arising from the presence of polydispersity in systems in which the particles interact with a hard-core soft repulsive Yukawa potential.

Experiments indicate that in systems of charge-stabilized colloidal particles suspended in apolar or low-polar solvents the charge on the colloids is packing-fraction-dependent.[9,37–40] The interactions in these HSY systems are therefore more accurately described by constant-potential boundary conditions than constant-charge boundary conditions.[38,39,41] Only recently, phase diagrams for HSY systems were calculated within the constant-potential model.[42] Use of the constant-potential model requires calculation of the packing-fraction-dependent effective colloidal charge and effective screening length. Because of these technical difficulties the present simulations were started with all particles having the same surface potential, but the amount of charge was not a function of the packing fraction or distance between the particles.

We used Monte Carlo simulations to study the effect of polydispersity on the behavior of hard-core Yukawa systems. It was found that Monte Carlo simulations in which physically relevant moves (small particle displacements) are used, are a correct and efficient way to investigate the dynamics in colloidal systems.[43–45] Molecular dynamics simulations are less appropriate to describe the dynamics in suspensions of colloidal particles, as they employ Newtonian dynamics rather than the Brownian dynamics which is operative in colloidal systems. We expect only limited fractionation, to the extent introduced by the selected initial configuration and allowed for by the diffusion of the particles on simulation timescales. We note that *NVT* Monte Carlo simulations are not a suitable technique to establish the equilibrium behavior of a polydisperse system, as was pointed out in Ref. 22. The behavior of the system at coexistence will be dominated by finite-size effects, which can be more severe in polydisperse systems compared to monodisperse systems, because in polydisperse systems some phases may occupy only a very small volume when the constituting particle sizes are under-represented in the overall size distribution. Furthermore, the use of fixed particle sizes in combination with slow diffusion, as is the case for our system, means that fractionation is very slow and on simulation timescales equilibrium is not reached. The results might be indicative of what could happen in an experiment in which a polydisperse system is allowed to crystallize at a

low packing fraction and is subsequently slowly compressed, for example, by gravity. For certain combinations of parameters sufficiently slow compression is expected to preserve the crystalline structure up to the packing fraction where the lattice spacing becomes too small to accommodate the spread of sizes present in a polydisperse system. The extent to which fractionation takes place will be determined by the mobility of the particles at this packing fraction. Slow dynamics will prevent the system to fully fractionate on experimental timescales, resulting in phase behavior that depends on the quenched polydispersity.

The remainder of this paper is organized in the following way. In Sec. II we give simulation details and describe the order parameters we used to analyze the results, in Sec. III we discuss the results, and in Sec. IV our conclusions are presented.

II. METHOD

A. Simulation details

In our model, the particles interact through a pairwise hard-core repulsive Yukawa potential:[46]

$$u_{ij}(r) = \begin{cases} \epsilon_{ij}\frac{\sigma_{ij}}{r}e^{-\kappa(r-\sigma_{ij})} & r \geq \sigma_{ij} \\ \infty & r < \sigma_{ij} \end{cases}, \tag{1}$$

with $\sigma_{ij} = (\sigma_i + \sigma_j)/2$ and the contact value of the potential between two colloids i and j

$$\beta\epsilon_{ij} = \frac{Z_i Z_j}{(1+\kappa\sigma_i/2)(1+\kappa\sigma_j/2)}\frac{\lambda_B}{\sigma_{ij}}, \tag{2}$$

where r is the center-to-center distance between particles i and j, Z_i (Z_j), and σ_i (σ_j) are the charge number and diameter of colloid i (j), $\lambda_B = e^2/(4\pi\epsilon_r\epsilon_0 k_B T)$ is the Bjerrum length (with e the unit charge, ϵ_r the relative dielectric constant of the solvent, ϵ_0 the dielectric permittivity of vacuum, k_B the Boltzmann constant, and T the absolute temperature), $\beta = 1/(k_B T)$, and $\kappa = \sqrt{8\pi\lambda_B\rho_s}$ is the inverse Debye screening length (with ρ_s the monovalent salt concentration). The electrostatic surface potential ψ_i for an isolated particle is given by[12]

$$\beta e\psi_i = \frac{Z_i}{1+\kappa\sigma_i/2}\frac{2\lambda_B}{\sigma_i}. \tag{3}$$

We took the charge number of the particles such that particles with a different size had the same surface potential. However, as mentioned before, the surface charge was not a function of the packing fraction or distance between the particles. This means that the charge number of particle i with diameter σ_i is given by

$$Z_i = Z\frac{\sigma_i}{\bar{\sigma}}\frac{1+\kappa\sigma_i/2}{1+\kappa\bar{\sigma}/2}, \tag{4}$$

where Z and $\bar{\sigma}$ are the charge number and diameter of a chosen reference particle. Inserting this expression for the charge number in Eq. (1) leads to the following expression for the potential:

$$u_{ij}(r) = \begin{cases} \bar{\epsilon}\frac{\sigma_i\sigma_j}{\bar{\sigma}r}e^{-\kappa(r-\sigma_{ij})} & r \geq \sigma_{ij} \\ \infty & r < \sigma_{ij} \end{cases}, \tag{5}$$

where $\beta\bar{\epsilon} = Z^2\lambda_B/[(1+\kappa\bar{\sigma}/2)^2\bar{\sigma}]$ is the contact value of the potential for two reference particles with charge number Z and diameter $\bar{\sigma}$ (see Eq. (2)).

The particle diameters σ in our systems are distributed according to a log-normal distribution:

$$p(\sigma;\mu,\delta) = \frac{1}{\sigma\delta\sqrt{2\pi}}e^{-\frac{(\ln\sigma-\mu)^2}{2\delta^2}}, \tag{6}$$

where μ and δ are the mean and the standard deviation of the natural logarithm of variable σ (which is a continuous variable, contrary to σ_i above). The diameter of the above-mentioned reference particle ($\bar{\sigma}$) is chosen such that $\mu = \ln\bar{\sigma}$. The use of a log-normal distribution rather than a Gaussian distribution avoids the problem of having a finite probability for negative diameters. We define the polydispersity s as the ratio of the standard deviation and the mean of σ:

$$s \equiv \frac{\sqrt{\langle\sigma^2\rangle - \langle\sigma\rangle^2}}{\langle\sigma\rangle}. \tag{7}$$

The polydispersity can be written in terms of the log-normal distribution parameter δ:

$$s = \sqrt{e^{\delta^2} - 1}, \tag{8}$$

and for the values of δ that we use ($\delta \in [0.00, 0.15]$), s can be approximated by

$$s \approx \delta. \tag{9}$$

We performed NVT Monte Carlo simulations, keeping the number of particles N, the volume of the cubic box V, and the absolute temperature T constant. The packing fraction η is given by

$$\eta = \frac{\pi}{6V}\sum_{i=1}^{N}\sigma_i^3, \tag{10}$$

where the sum runs over all particles N in the system and σ_i is the diameter of particle i. The initial configuration was either a face-centered-cubic (fcc; $N = 2048$) or body-centered-cubic (bcc; $N = 2000$) crystal configuration, chosen to match the stable crystalline phase of the monodisperse system at the packing fraction of the crystal-fluid transition, as determined from free energy calculations in Monte Carlo simulations.[4] Polydisperse initial configurations were made by placing N particles on a crystal lattice with diameters randomly assigned according to the aforementioned log-normal distribution. If overlap occurred each particle was assigned a new diameter. For each combination of $\beta\bar{\epsilon}$, $\kappa\bar{\sigma}$, η, and s we made not more than 10^6 attempts at generating non-overlapping configurations. It should be noted that above a certain polydispersity this procedure does not result in non-overlapping initial configurations. We used two different typical contact values, $\beta\bar{\epsilon} = 20$ and 81 (corresponding to surface potentials $\psi_0 \approx 23$ and 46 mV at room temperature, assuming $\lambda_B/\bar{\sigma} \approx 0.01$), and several values of $\kappa\bar{\sigma}$ from the range 2.5–10. The pair potential was cut off at a distance of $4.10\bar{\sigma}$. We found no significant differences in our results for larger values of this cut-off distance. The maximum displacement

of the particles was set to $0.1\bar{\sigma}$. Simulations were run for 2×10^4 Monte Carlo cycles, where one cycle means on average one displacement per particle. For each state point five independent runs were performed. After 2×10^4 Monte Carlo cycles we analyzed the configurations by calculating various order parameters (see Sec. II B).

B. Order parameters

For each particle i we can define a set of $2l + 1$ bond-orientational order parameters $q_{lm}(i)$:

$$q_{lm}(i) = \frac{1}{N_b(i)} \sum_{j=1}^{N_b(i)} Y_{lm}(\theta_{ij}, \phi_{ij}), \tag{11}$$

where $N_b(i)$ is the number of neighbors of particle i, θ_{ij}, and ϕ_{ij} are the inclination and azimuth angles of the bond $\mathbf{r}_{ij} = \mathbf{r}_i - \mathbf{r}_j$ (where $\mathbf{r}_i$ ($\mathbf{r}_j$) denotes the position of particle i (j)) connecting the centers of particle i and its neighbor j, and $Y_{lm}(\theta_{ij}, \phi_{ij})$ are the spherical harmonics with $m \in [-l, l]$. The neighbors of particle i are defined as all particles within a certain cut-off distance r_c from particle i.

We used these sets of bond-orientational order parameters to calculate three different order parameters. The local bond-orientational order parameter $q_l(i)$ is calculated in the following way:[47]

$$q_l(i) = \sqrt{\frac{4\pi}{2l+1} \sum_{m=-l}^{l} |q_{lm}(i)|^2}, \tag{12}$$

where $q_{lm}(i)$ is defined in Eq. (11). We can average each of the members of the set from Eq. (11) over the central particle and its neighbors, to obtain for each particle i a set of *averaged* bond-orientational order parameters $\bar{q}_{lm}(i)$:

$$\bar{q}_{lm}(i) = \frac{1}{N_b(i)+1} \sum_{j=0}^{N_b(i)} q_{lm}(j), \tag{13}$$

where the sum runs over all the neighbors of particle i plus the particle i itself. From these sets of averaged bond-orientational order parameters, we obtain an averaged local bond-orientational order parameter $\bar{q}_l(i)$:[48]

$$\bar{q}_l(i) = \sqrt{\frac{4\pi}{2l+1} \sum_{m=-l}^{l} |\bar{q}_{lm}(i)|^2}. \tag{14}$$

Finally, the correlation between the sets of bond-orientational order parameters for each pair of neighboring particles can be written as

$$c_l(ij) = \frac{\sum_{m=-l}^{l} q_{lm}(i) q^*_{lm}(j)}{\left(\sum_{m=-l}^{l} |q_{lm}(i)|^2\right)^{1/2} \left(\sum_{m=-l}^{l} |q_{lm}(j)|^2\right)^{1/2}}, \tag{15}$$

where $q_{lm}(i)$ is defined in Eq. (11) and $q^*_{lm}(j)$ is the complex conjugate of $q_{lm}(j)$. Crystalline particles are defined as particles with more than a certain number n_c of connected neighbors, where a connected neighbor is a neighbor j to particle i for which $c_l(ij)$ exceeds a threshold value c_c.[49] For our analysis we chose $l = 6$, $r_c = 1.5\rho^{-1/3}$ (with $\rho = N/V$ the number density of the particles, and $\rho^{-1/3}$ the characteristic interparticle distance), $c_c = 0.6$, and $n_c = 8$. We use this order parameter for calculating the fraction of crystalline particles in the system (the crystalline fraction is 1.0 in a perfect bulk fcc or bcc crystal, and close to 0.0 in a fluid), and for calculating the average crystallinity of a particle during a part of the simulation, which is the fraction of time that the particle is crystalline during that part of the simulation.

In order to determine whether certain arrangements of particles were liquid or glassy we also looked at particle dynamics, without taking interparticle hydrodynamic effects into account, as measured by particle diffusion. The mean square displacement from the initial (ideal) lattice positions at a certain point τ in the simulation is given by

$$\langle \Delta r(\tau)^2 \rangle = \frac{1}{N} \sum_{i=1}^{N} (\mathbf{r}_i(\tau) - \mathbf{r}_i(0))^2, \tag{16}$$

where $\mathbf{r}_i(\tau)$ is the position of particle i at time τ and $\mathbf{r}_i(0)$ the initial (ideal) lattice position of particle i.

III. RESULTS AND DISCUSSION

We studied the following combinations of the Yukawa potential parameters: for the weakly charged particles with reference contact value $\beta\bar{\epsilon} = 20$ we studied $\kappa\bar{\sigma}$-values in the range 3.3–10, corresponding to screening lengths $(\kappa\bar{\sigma})^{-1}$ in the range 0.30–0.10; for the more highly charged particles with $\beta\bar{\epsilon} = 81$ we studied $\kappa\bar{\sigma}$-values in the range 2.5–10, corresponding to screening lengths $(\kappa\bar{\sigma})^{-1}$ in the range 0.40–0.10. In Fig. 1 we plotted some of the pair potentials for two reference particles with diameter $\bar{\sigma}$. For each polydispersity, we calculated the crystalline fraction and the mean square displacement from the initial lattice positions over a range of packing fractions. We found qualitatively different behavior for the weakly and more highly charged particles; below we will discuss the results for both.

A. Weakly charged particles

First we consider the case of weakly charged particles ($\psi_0 \approx 23$ mV). Despite their low surface potential, parti-

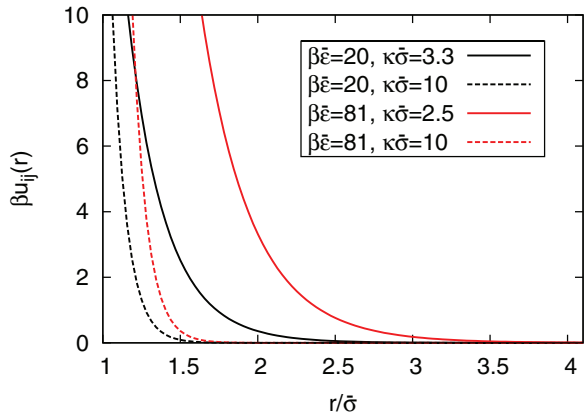

FIG. 1. Pair potentials for two reference particles with diameter $\bar{\sigma}$ for four different combinations of Yukawa potential parameters $\beta\bar{\epsilon}$ and $\kappa\bar{\sigma}$.

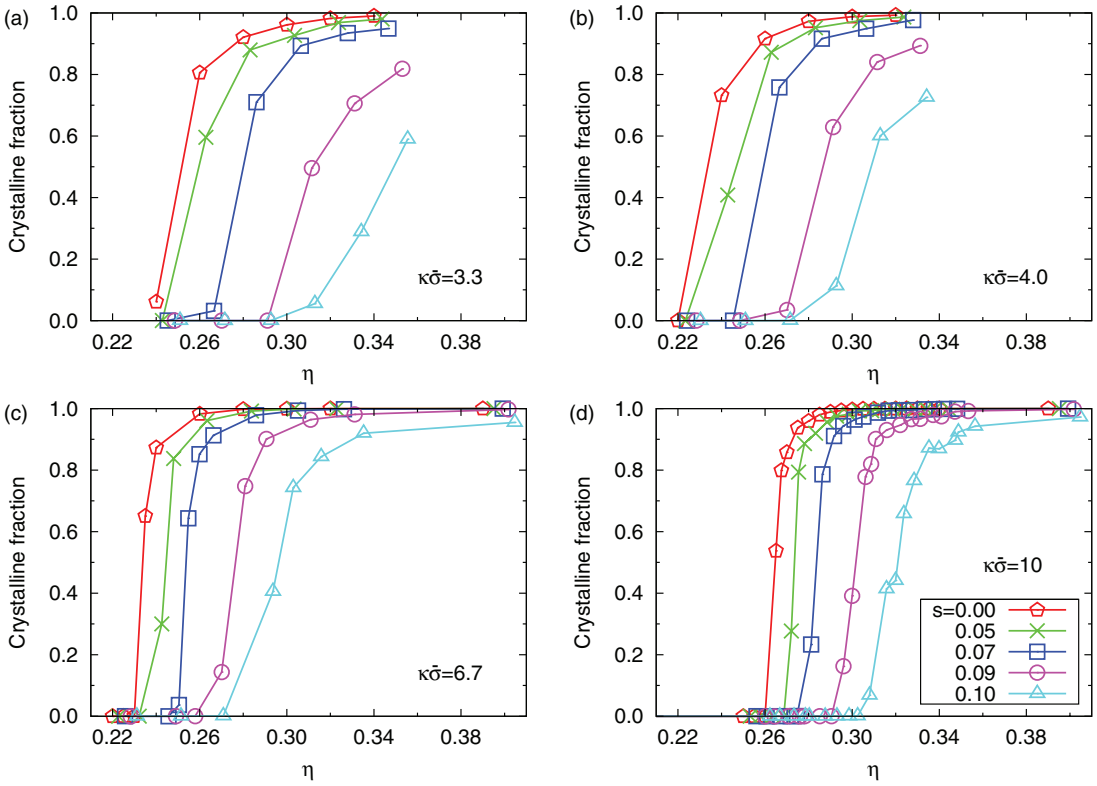

FIG. 2. Crystalline fraction versus packing fraction η of a system of particles which interact with a hard-core repulsive Yukawa pair potential with reference contact value $\beta\bar{\epsilon} = 20$ and (a) $\kappa\bar{\sigma} = 3.3$, (b) 4.0, (c) 6.7, and (d) 10 after a simulation of 2×10^4 Monte Carlo cycles, starting from a bcc ($\kappa\bar{\sigma} = 3.3$ and 4.0) or fcc ($\kappa\bar{\sigma} = 6.7$ and 10) crystal structure, for different polydispersities s in the range 0.00–0.10 as labeled.

cles will hardly ever come into contact with their hard cores, as the size of the particles makes that $\beta\bar{\epsilon} = 20$. Figure 2 presents the crystalline fraction versus packing fraction for $\kappa\bar{\sigma} = 3.3$, 4.0, 6.7, and 10. We started our simulation with a bcc phase for $\kappa\bar{\sigma} = 3.3$ and 4.0, while an fcc phase was used for $\kappa\bar{\sigma} = 6.7$ and 10, chosen to match the stable crystalline phase of the monodisperse system at the packing fraction of the crystal-fluid transition.[4] Due to hysteresis the crystal-fluid transition for the monodisperse system $\eta_{\mathrm{CF}}(0)$ was found at slightly lower packing fraction than in the equilibrium phase diagram, e.g., for $\kappa\bar{\sigma} = 3.3$ we find $\eta_{\mathrm{CF}}(0) \approx 0.26$ versus $\eta_{\mathrm{CF}}(0) \approx 0.28$ in the phase diagram obtained from free energy calculations using Monte Carlo simulations.[4,32] Hysteresis was also found for the polydisperse systems with $\kappa\bar{\sigma} = 3.3$ and 10, when comparing to results on systems with very similar potential parameters from Ref. 32. For systems with polydispersity above 0.10 (values tried were 0.13 and 0.15) it was not possible to obtain a fully crystalline starting configuration within a reasonable number of attempts. From the plots in Fig. 2 we see that the crystal-fluid transition shifts to higher packing fractions with increasing polydispersity. This shift is present for all $\kappa\bar{\sigma}$-values in the range 3.3–10, but the shift is larger if the particles are softer (smaller $\kappa\bar{\sigma}$ or larger screening length $(\kappa\bar{\sigma})^{-1}$). To illustrate this, we plotted in Fig. 3 for four different $\kappa\bar{\sigma}$-values the shift in packing fraction, defined as

$$\Delta\eta(s) = \eta_{\mathrm{CF}}(s) - \eta_{\mathrm{CF}}(0), \tag{17}$$

where $\eta_{\mathrm{CF}}(s)$ and $\eta_{\mathrm{CF}}(0)$ are the packing fraction of the crystal-fluid transition for polydispersity s and for the monodisperse system (with $s = 0$), respectively. We took for $\eta_{\mathrm{CF}}(s)$ and $\eta_{\mathrm{CF}}(0)$ the values of the packing fraction at which the (interpolated) crystalline fraction equals 0.80. From Fig. 3 it is clear that the shift of the crystal-fluid transition with increasing polydispersity is larger for softer particles. The initial crystal type (bcc or fcc) does not appear to qualitatively influence the shift. We assume that a packing frac-

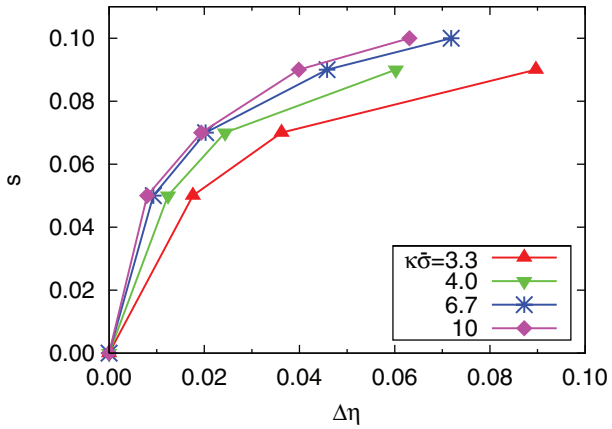

FIG. 3. Shift in packing fraction of the crystal-fluid transition $\Delta\eta(s)$ (as defined in Eq. (17)) with size polydispersity s of a system of hard-core repulsive Yukawa particles with reference contact value $\beta\bar{\epsilon} = 20$ and $\kappa\bar{\sigma} = 3.3$, 4.0, 6.7, and 10 as labeled.

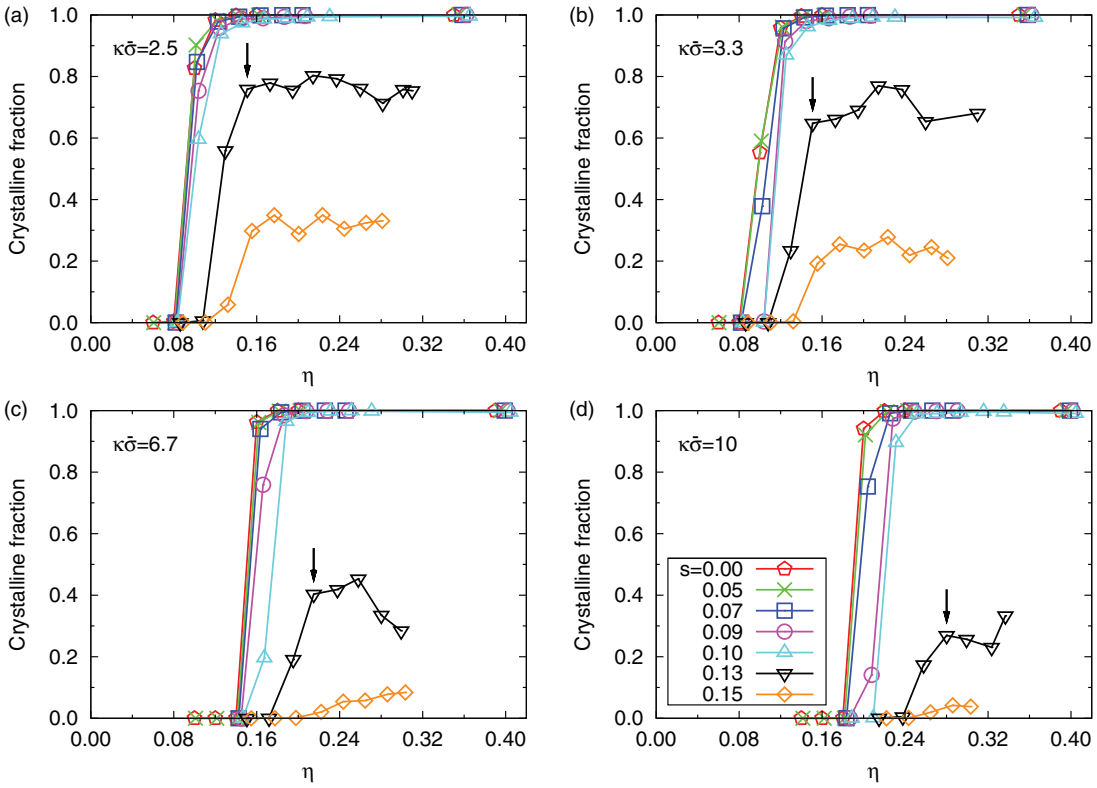

FIG. 4. Crystalline fraction versus packing fraction η of a hard-core repulsive Yukawa system with reference contact value $\beta\bar{\epsilon} = 81$ and (a) $\kappa\bar{\sigma} = 2.5$, (b) 3.3, (c) 6.7, and (d) 10 after a simulation of 2×10^4 Monte Carlo cycles, starting from a bcc ($\kappa\bar{\sigma} = 2.5$ and 3.3) or fcc ($\kappa\bar{\sigma} = 6.7$ and 10) crystal structure, for different polydispersities s in the range 0.00–0.15 as labeled. The arrows indicate the edge of the plateau for $s = 0.13$ and may be used for comparison with Figs. 7 and 8.

tion corresponding to a crystalline fraction of 0.80 lies in the coexistence gap and take it as a measure for the packing fraction at which the crystal-fluid transition would occur in quenched equilibrium where fractionation is not allowed for. We wish to remark here that different simulation techniques that allow for fractionation are required to determine the equilibrium phase behavior of polydisperse systems (see, e.g., Refs. 22, 23, 50, and 51). It is tempting to speculate that a longer-range potential gives rise to a larger effective polydispersity, which would explain the larger shift of the crystal-fluid packing fraction with polydispersity.

B. More highly charged particles

Figure 4 shows the crystalline fraction versus packing fraction for more highly charged particles ($\psi_0 \approx 46$ mV) with $\beta\bar{\epsilon} = 81$ and $\kappa\bar{\sigma} = 2.5$, 3.3, 6.7, and 10. We started our simulation with a bcc phase for $\kappa\bar{\sigma} = 2.5$ and 3.3, while an fcc phase was used for $\kappa\bar{\sigma} = 6.7$ and 10, chosen to match the stable crystalline phase of the monodisperse system at the packing fraction of the crystal-fluid transition.[4] Comparing these plots to Fig. 2 for $\beta\bar{\epsilon} = 20$, we see a much weaker shift in the crystal-fluid transition with increasing polydispersity. Up to $s = 0.10$ we hardly see a shift at all, while for higher polydispersities the shift, if present, is much smaller than in the case of weakly charged particles. For the weakly charged particles melting takes place at relatively high packing fraction; the characteristic interparticle distance at the crystal-fluid transition is thus smaller than for the more highly charged particles. It seems likely that for the case of weakly charged particles, the crystal lattice can therefore not accommodate an equally broad spread in sizes as for the case of more highly charged particles, which seems a possible reason for the larger shift of the crystal-fluid packing fraction for the case of weakly charged particles.

The crystal-fluid transition for $\beta\bar{\epsilon} = 81$ occurred at lower packing fractions than for $\beta\bar{\epsilon} = 20$, which allowed us to investigate higher polydispersities and higher packing fractions relative to the packing fraction of the monodisperse crystal-fluid transition. In this region we observed something not found for the weakly charged systems: for $s = 0.13$ and 0.15 only parts of the system became disordered, while the remaining parts stayed crystalline. After running the simulations for 2×10^5 cycles (ten times the length of the initial run) the crystalline fraction for $s = 0.13$ was still at the same value, and the crystalline fraction for $s = 0.15$ had only slightly decreased (for analysis confirming that the disordered parts did not display long-time self-diffusion and hence were not fluid, see below). The crystalline fraction at which the system seems to stabilize is lower for higher polydispersity (e.g., for $\kappa\bar{\sigma} = 2.5$ this crystalline fraction is ~0.80 for $s = 0.13$ and ~0.30 for $s = 0.15$), but is for a given polydispersity approximately the same over a whole range of packing fractions. For all other $\kappa\bar{\sigma}$-values we observed the same phenomenon, with the crystalline fraction at which the system

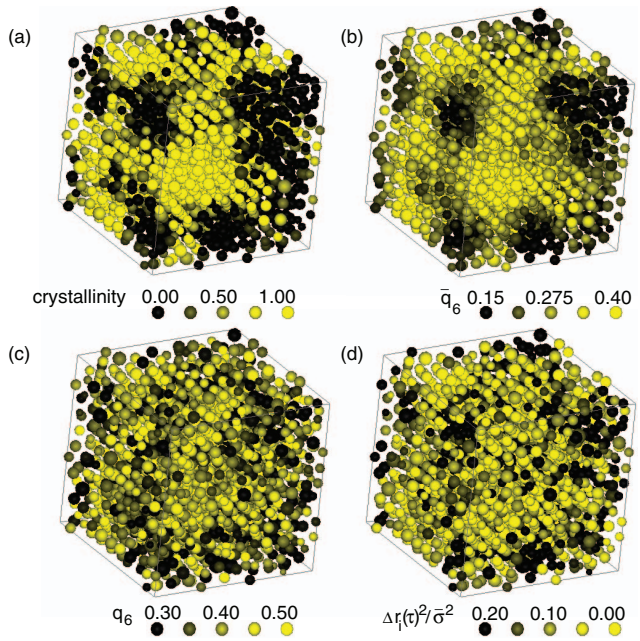

FIG. 5. Snapshot after 2×10^4 Monte Carlo cycles of a hard-core repulsive Yukawa system with reference contact value $\beta\bar{\epsilon} = 81$, $\kappa\bar{\sigma} = 2.5$, $\eta = 0.20$, and $s = 0.15$. The color of a particle indicates (a) the average crystallinity in a series of six configurations between 1.5×10^4 and 2×10^4 Monte Carlo cycles, (b) the average local bond-orientational order parameter $\bar{q}_6(i)$ (Eq. (14)) after 2×10^4 MC cycles, (c) local bond-orientational order parameter $q_6(i)$ (Eq. (12)) after 2×10^4 MC cycles, and (d) the square displacement from the particle's ideal lattice position $\Delta r_i(\tau)^2/\bar{\sigma}^2 = (\mathbf{r}_i(\tau) - \mathbf{r}_i(0))^2/\bar{\sigma}^2$ for $\tau = 2 \times 10^4$ Monte Carlo cycles.

stabilizes decreasing with increasing $\kappa\bar{\sigma}$ to ~0.25 and ~0.05, respectively, for $s = 0.13$ and 0.15 (for $\kappa\bar{\sigma} = 10$).

We took a closer look at several of the configurations where the crystalline fraction reached a plateau for a range of packing fractions. Figure 5 shows four times the same snapshot after 2×10^4 cycles of a configuration with $\beta\bar{\epsilon} = 81$, $\kappa\bar{\sigma} = 2.5$, $s = 0.15$, and $\eta = 0.20$. For Fig. 5(a) we calculated the crystallinity for each particle as described in Sec. II for a series of six configurations between 1.5×10^4 and 2×10^4 Monte Carlo cycles (crystallinity = 1 for a crystalline particle, 0 for a non-crystalline particle) and determined the average crystallinity; black particles have low crystallinity, while yellow (light gray) particles have high crystallinity. In Fig. 5(b) each particle's color indicates for the configuration after 2×10^4 cycles whether its average local bond-orientational order parameter $\bar{q}_6$ is low (black) or high (yellow/light gray). In Fig. 5(c) we show the same, but for the non-averaged local bond-orientational order parameter q_6. In the fourth snapshot, Fig. 5(d), a particle's color is determined by the square of the displacement $\Delta r_i(\tau)^2 = (\mathbf{r}_i(\tau) - \mathbf{r}_i(0))^2$ from its ideal initial lattice position: small (black) or large (yellow/light gray).

From the average crystallinity of each particle (Fig. 5(a)) we see that in this snapshot, and also the other snapshots we looked at, the crystalline particles and non-crystalline particles are in different domains. We observed strong correlation between the average crystallinity and the average local order parameter $\bar{q}_6$ of each particle: Fig. 5(b) shows similar domains. Less correlation is found between the average crystallinity and the non-averaged local bond-orientational order parameter q_6: there are large fluctuations in the value of q_6 within a domain (Fig. 5(c)). This means that an individual particle within an ordered domain does not necessarily have a high q_6 itself. However, the probability of finding a particle with a high q_6-value is higher in a domain consisting of particles with high average crystallinity and high $\bar{q}_6$. The correlation between the square displacement $\Delta r_i(\tau)^2$ and average crystallinity is present, but also not very strong: the *mean* square displacement $\langle \Delta r(\tau)^2 \rangle$ (Eq. (16)) is smaller in crystalline domains than non-crystalline domains, but we find large fluctuations in the square displacement $\Delta r_i(\tau)^2$ of individual particles within a domain.

C. Terminal polydispersity

We determined three size distributions for the final configuration of each run (after 2×10^4 MC cycles): one for the total system, a second for the most-disordered particles, and a third for the most-ordered particles. Particles are labeled "most-disordered" or "most-ordered" by calculating the average crystallinity as described in Sec. II. A most-disordered particle is crystalline in at most one out of six configurations and a most-ordered particle in at least five out of six configurations between 1.5×10^4 and 2×10^4 Monte Carlo cycles. The diameters were sampled from a continuous log-normal distribution; the calculated polydispersities for the sampled size distributions for the total system were very close to (within ~1% from) the polydispersity of the continuous distribution.

In Fig. 6 we plotted the three size distributions averaged over five simulations (for better statistics) with $\beta\bar{\epsilon} = 81$, $\kappa\bar{\sigma} = 2.5$, $s = 0.15$, and $\eta = 0.20$. The most-disordered size distribution (dashed red line) has a peak slightly, but significantly, more to the left (at smaller size) than the most-ordered size distribution (solid blue line). The most-disordered size distribution is also broader (has a higher polydispersity) than the most-ordered size distribution. Size distributions for

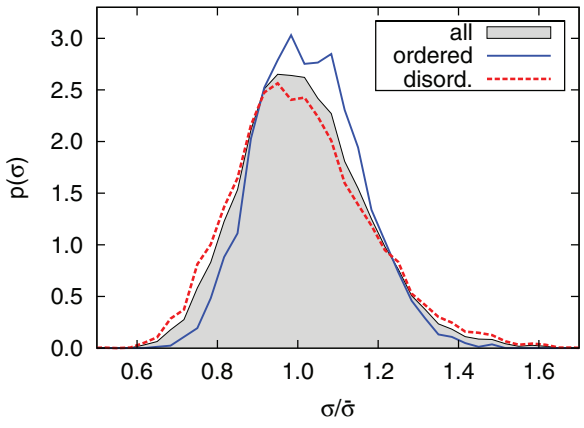

FIG. 6. Normalized probability distribution functions $p(\sigma)$ of the particle diameter σ for $\beta\bar{\epsilon} = 81$, $\kappa\bar{\sigma} = 2.5$, $s = 0.15$, and $\eta = 0.20$ (55% most-disordered particles, 25% most-ordered particles). Filled gray curve: all particles, solid blue line: most-ordered particles (particles that are crystalline in at least five out of six configurations between 1.5×10^4 and 2×10^4 Monte Carlo cycles), dashed red line: most-disordered particles (particles that are crystalline in at most one out of six configurations between 1.5×10^4 and 2×10^4 Monte Carlo cycles).

configurations at different packing fractions show similar characteristics, as do the distributions for $s = 0.13$. Probably, local differences in polydispersity determine whether the system stays crystalline or becomes disordered, with a higher local polydispersity destabilizing the crystal structure and causing the system to become locally disordered.

Whether a configuration is disordered or crystalline depends on our definitions; however, it is clear that above a certain polydispersity a long-range ordered configuration or crystal cannot be formed regardless of the definition. If the system had time to fractionate this is presumably what would eventually happen; however, given the slow dynamics in solid and glassy states, it is probably still useful to determine a value of the quenched polydispersity, i.e., with no fractionation taken into account, above which crystallization does not occur. It should be kept in mind that the way the initial crystal configurations are chosen can also be seen as selecting systems that are already slightly fractionated.

In a system with a higher polydispersity a larger part of the configuration is locally destabilized by fluctuations in the polydispersity, which explains why we find a larger fraction of disordered particles in the configurations with $s = 0.15$ than in the configurations with $s = 0.13$. As mentioned above, the crystalline fraction at which the system stabilizes is for a given polydispersity approximately the same over a range of packing fractions. This can be explained if we note that the fraction of particles in the system that experiences the local polydispersity to be larger than some terminal polydispersity (and therefore becomes disordered) is independent of the packing fraction in the system, and assume that significant reentrant melting does not yet happen in this range of packing fractions.

To verify this explanation further, we calculated the polydispersity for the most-disordered and most-ordered particles in the systems with overall polydispersity $s = 0.13$ and 0.15. For the final configuration of each run (after 2×10^4 MC cycles) we calculated the polydispersity of the size distribution for the most-disordered particles and the polydispersity of the size distribution for the most-ordered particles. We averaged for each state point the obtained polydispersity values for the five independent runs. The results are shown in Fig. 7, where we plotted, for overall polydispersity $s = 0.13$, the polydispersity versus packing fraction in the total system, in the most-disordered parts and in the most-ordered parts of the system. The polydispersity in the most-ordered parts is significantly lower than in the most-disordered parts. We also note that the polydispersities in the most-ordered and most-disordered parts of the system are similar over the range of packing fractions for which the system seems to stabilize at a certain crystalline fraction (i.e., the range of packing fractions where the plot for $s = 0.13$ in Fig. 4 forms a plateau). For systems with $s = 0.15$ we find for the polydispersity of the most-ordered particles values similar to those for systems with $s = 0.13$.

The polydispersity of the most-ordered parts can be regarded as a measure for the terminal polydispersity, since the homogeneous crystal phase is no longer stable if the local polydispersity of the system is higher than this value. This terminal polydispersity decreases with increasing $\kappa\bar{\sigma}$ from $\sim$0.12 for $\kappa\bar{\sigma} = 2.5$ to $\sim$0.105 for $\kappa\bar{\sigma} = 10$. We expect softer

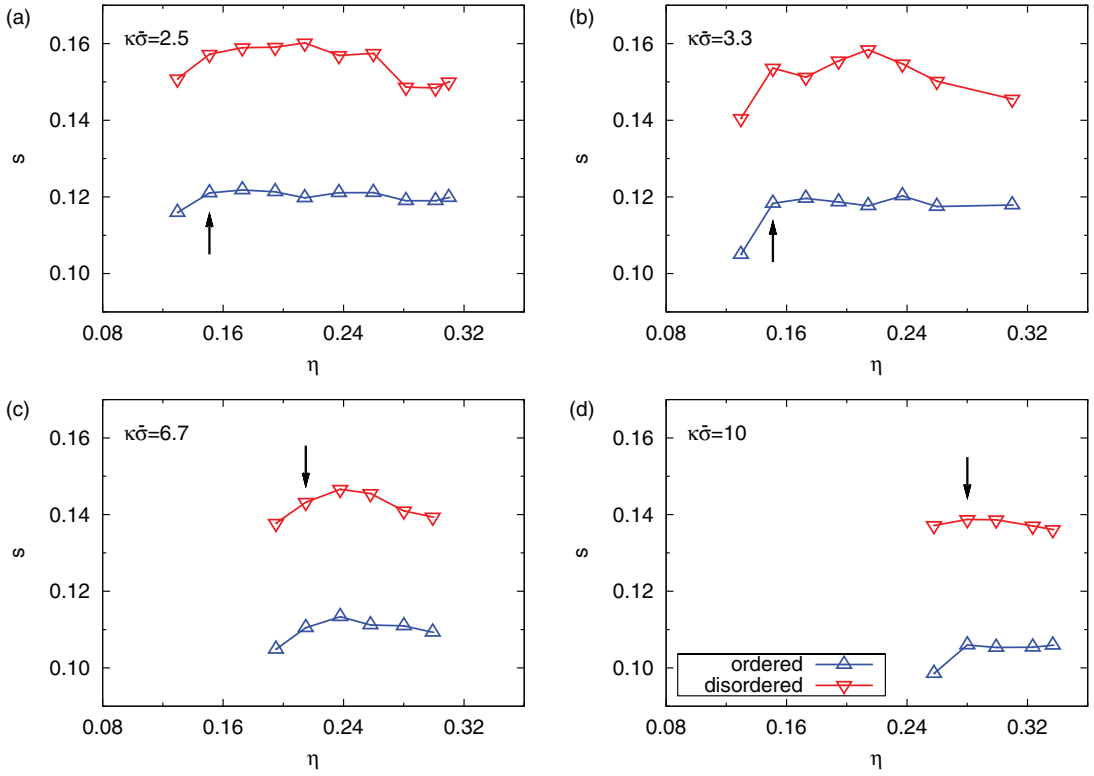

FIG. 7. Polydispersity s versus packing fraction η of the most-ordered and most-disordered parts of hard-core repulsive Yukawa systems with reference contact value $\beta\bar{\epsilon} = 81$ and an overall polydispersity $s = 0.13$. For (a) $\kappa\bar{\sigma} = 2.5$, (b) 3.3, (c) 6.7, and (d) 10 after a simulation of 2×10^4 Monte Carlo cycles, starting from a bcc ($\kappa\bar{\sigma} = 2.5$ and 3.3) or fcc ($\kappa\bar{\sigma} = 6.7$ and 10) crystal structure. The arrows indicate the same state points as in Fig. 4.

particles (with $\kappa\bar{\sigma} < 2.5$) to have an even higher terminal polydispersity. These values are in good agreement with the estimated terminal polydispersity ($0.125 < s < 0.13$ for parameters close to $\beta\bar{\epsilon} = 81$ and $\kappa\bar{\sigma} = 3.3$) as obtained from free energy calculations.[32] We take the trend observed for our values for the terminal polydispersity as an indication of what might be found for more reliable terminal polydispersities that could be measured using simulations that can achieve equilibrium.[22]

D. Slow dynamics

Figure 8 shows the mean square displacement from the initial ideal lattice positions versus packing fraction for $\beta\bar{\epsilon} = 81$, $\kappa\bar{\sigma} = 2.5$, and a range of polydispersities s. From this plot we see that in all systems that stay completely or partly crystalline, particles do not move over a distance larger than the typical particle diameter during the length of the simulation. This means that the dynamics in the system does not allow for local fluctuations in the polydispersity to change during the simulation and that the disordered parts in these systems are therefore essentially glassy, i.e., the particles display no long-time self-diffusion and are disordered. This is illustrated further in Fig. 9, which shows the trajectories for 25 neighboring particles during a simulation of 2×10^5 cycles for the state point with $\beta\bar{\epsilon} = 81$, $\kappa\bar{\sigma} = 2.5$, $s = 0.15$, and $\eta = 0.20$. Most particles are confined to the cage formed by their neighbors during the length of the simulation, whereby some stay on their lattice position, while others are moved from their original position due to local distortion of the lattice. A few particles move from their lattice point and displace one of their neighbors, which then in turn hops to the lattice point of another neighbor or simply becomes part of a disordered part of the system. Most of these hopping movements and lattice distortions seem to occur early in the simulation, which is consistent with the observation that increasing the simulation length from 2×10^4 to 2×10^5 cycles does not significantly change the crystalline fraction in the system.

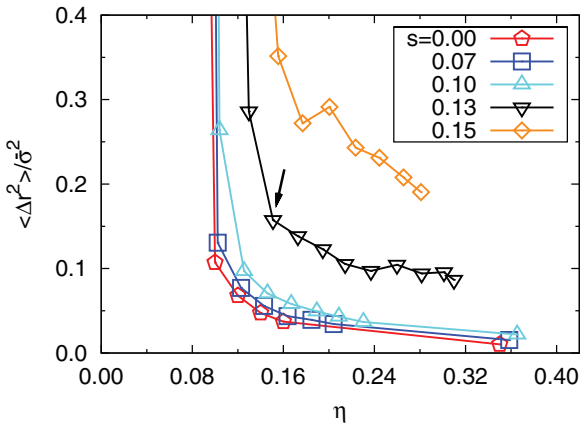

FIG. 8. Mean square displacement $\langle \Delta r(\tau)^2 \rangle$ from the ideal lattice position (Eq. (16)) versus packing fraction η for reference contact value $\beta\bar{\epsilon} = 81$ and $\kappa\bar{\sigma} = 2.5$ after a simulation of 2×10^4 Monte Carlo cycles, starting from a bcc crystal structure, for different polydispersities s in the range 0.00–0.15 as labeled. The arrow indicates the same state point as in Fig. 4(a).

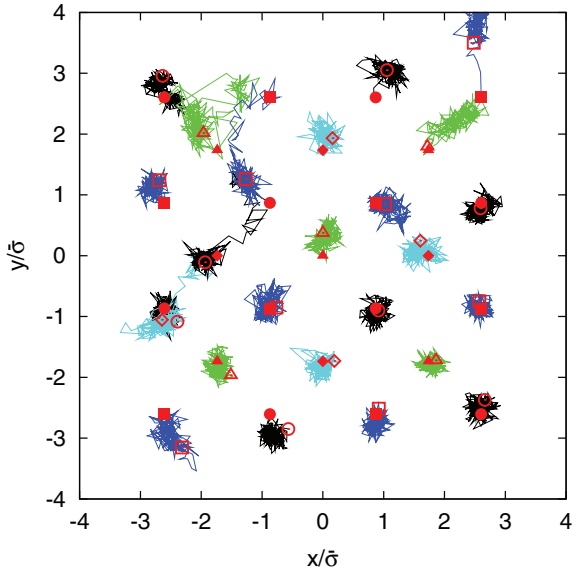

FIG. 9. 2D projections of 3D trajectories during 2×10^5 Monte Carlo cycles of 25 particles from a configuration with $\beta\bar{\epsilon} = 81$, $\kappa\bar{\sigma} = 2.5$, $s = 0.15$, and $\eta = 0.20$. The initial configuration is a perfect bcc crystal; the initial positions of the particles are indicated by *solid* red symbols. Initially, the 25 particles are in two parallel {100} planes: 16 particles (solid red circles and solid red squares) in one plane occupy the corners of 3×3 unit cells, 9 particles (solid red triangles and solid red diamonds) in the second plane are in the centers of the unit cells. The end positions after 2×10^5 MC cycles are indicated by *empty* red symbols (again circles, squares, triangles and diamonds; for each particle we used a symbol of the same shape to indicate the initial and end position). The trajectories are shown with four different colours (black, blue, green, and cyan, which correspond to the circles, squares, triangles, and diamonds, respectively).

IV. CONCLUSION

We investigated the effect of size polydispersity on the crystal-fluid transition in hard-core repulsive Yukawa systems. We observe a shift to higher packing fraction of the crystal-fluid transition of bulk crystals upon increasing the polydispersity, which is more pronounced for weakly charged particles ($\beta\bar{\epsilon} = 20$) compared to more highly charged particles ($\beta\bar{\epsilon} = 81$), and also for larger Debye screening length. For $\beta\bar{\epsilon} = 81$ at high polydispersities ($s \geq 0.13$; values used: $s = 0.13$ and 0.15) and high packing fractions, parts of the system that were initially crystalline became amorphous, indicating for these systems a terminal polydispersity beyond which the homogeneous crystal phase was no longer stable. For $\beta\bar{\epsilon} = 20$ we could not obtain crystalline systems for $s = 0.13$ and 0.15 for the packing fraction range of interest, providing a more direct indication that these values are above the terminal polydispersity.

We did not explicitly allow for size fractionation of the system other than the fractionation that "naturally" occurred within the system, although it should be kept in mind that the way the initial crystal configurations are chosen can also be seen as selecting systems that are already slightly fractionated. Due to the rather slow dynamics, we can only observe an onset to further fractionation because of the way the starting configuration was selected: the size distribution for "most-ordered" particles was narrower than the overall (imposed) size distribution. Note, that this is precisely the situation that

prevails in experimental systems: as in our simulations, the size distribution imposed by the particle synthesis can only fractionate to the extent allowed for by the system's dynamics. In this sense, the simulations closely resemble the experimental situation.

Free energy calculations in which fractionation is included, could give a better insight in the equilibrium phases of the hard-core repulsive Yukawa system. Those have been performed for the case of hard spheres, but not yet for the softer Yukawa system, which is more difficult to probe due to its much larger parameter space.

ACKNOWLEDGMENTS

The authors acknowledge financial support from the Netherlands Organisation for Scientific Research (NWO) through a Vici Grant (MD) and Toptalent Grant (MNvdL).

[1]W. B. Russel, D. A. Saville, and W. R. Schowalter, *Colloidal Dispersions* (Cambridge University Press, Cambridge, 1992).
[2]E. J. Meijer and F. El Azhar, J. Chem. Phys. **106**, 4678 (1997).
[3]F. El Azhar, M. Baus, J.-P. Ryckaert, and E. J. Meijer, J. Chem. Phys. **112**, 5121 (2000).
[4]A.-P. Hynninen and M. Dijkstra, Phys. Rev. E **68**, 021407 (2003).
[5]Y. Monovoukas and A. P. Gast, J. Colloid Interface Sci. **128**, 533 (1989).
[6]E. B. Sirota, H. D. Ou-Yang, S. K. Sinha, P. M. Chaikin, J. D. Axe, and Y. Fujii, Phys. Rev. Lett. **62**, 1524 (1989).
[7]C. P. Royall, M. E. Leunissen, and A. van Blaaderen, J. Phys.: Condens. Matter **15**, S3581 (2003).
[8]A. Yethiraj and A. van Blaaderen, Nature (London) **421**, 513 (2003).
[9]C. P. Royall, M. E. Leunissen, A.-P. Hynninen, M. Dijkstra, and A. van Blaaderen, J. Chem. Phys. **124**, 244706 (2006).
[10]P. Wette, I. Klassen, D. Holland-Moritz, D. M. Herlach, H. J. Schöpe, N. Lorenz, H. Reiber, T. Palberg, and S. V. Roth, J. Chem. Phys. **132**, 131102 (2010).
[11]P. Sollich, J. Phys.: Condens. Matter **14**, R79 (2002).
[12]R. J. Hunter, *Zeta Potential in Colloid Science. Principles and Applications* (Academic Press, London, 1981).
[13]P. N. Pusey, J. Phys. **48**, 709 (1987).
[14]R. McRae and A. D. J. Haymet, J. Chem. Phys. **88**, 1114 (1988).
[15]S.-E. Phan, W. B. Russel, J. Zhu, and P. M. Chaikin, J. Chem. Phys. **108**, 9789 (1998).
[16]P. Bartlett and P. B. Warren, Phys. Rev. Lett. **82**, 1979 (1999).
[17]D. A. Kofke and P. G. Bolhuis, Phys. Rev. E **59**, 618 (1999).
[18]M. Fasolo and P. Sollich, Phys. Rev. E **70**, 041410 (2004).
[19]P. Chaudhuri, S. Karmakar, C. Dasgupta, H. R. Krishnamurthy, and A. K. Sood, Phys. Rev. Lett. **95**, 248301 (2005).
[20]E. Zaccarelli, C. Valeriani, E. Sanz, W. C. K. Poon, M. E. Cates, and P. N. Pusey, Phys. Rev. Lett. **103**, 135704 (2009).
[21]P. Sollich and N. B. Wilding, Phys. Rev. Lett. **104**, 118302 (2010).
[22]N. B. Wilding and P. Sollich, J. Chem. Phys. **133**, 224102 (2010).
[23]P. Sollich and N. B. Wilding, Soft Matter **7**, 4472 (2011).
[24]E. Dickinson and R. Parker, J. Phys. Lett. **46**, 229 (1985).
[25]R. S. Farr and R. D. Groot, J. Chem. Phys. **131**, 244104 (2009).
[26]P. N. Pusey and W. van Megen, Nature (London) **320**, 340 (1986).
[27]P. N. Pusey, in *Liquids, Freezing and the Glass Transition*, edited by J. P. Hansen, D. Levesque, and J. Zinn-Justin (North-Holland, Amsterdam, 1991), Chap. 10.
[28]R. P. A. Dullens and W. K. Kegel, Phys. Rev. Lett. **92**, 195702 (2004).
[29]P. Yunker, Z. Zhang, and A. G. Yodh, Phys. Rev. Lett. **104**, 015701 (2010).
[30]B. V. R. Tata and A. K. Arora, J. Phys.: Condens. Matter **4**, 7699 (1992).
[31]M. Yiannourakou, I. G. Economou, and I. A. Bitsanis, J. Chem. Phys. **130**, 194902 (2009).
[32]J. Colombo and M. Dijkstra, J. Chem. Phys. **134**, 154504 (2011).
[33]S. Auer and D. Frenkel, Nature (London) **413**, 711 (2001).
[34]L. A. Fernández, V. Martín-Mayor, and P. Verrocchio, Phys. Rev. Lett. **98**, 085702 (2007).
[35]M. E. Leunissen and A. van Blaaderen, J. Chem. Phys. **128**, 164509 (2008).
[36]M. E. Leunissen, "Manipulating colloids with charges & electric fields," Ph.D. dissertation (Utrecht University, The Netherlands, 2007).
[37]M. Raşa and A. P. Philipse, Nature (London) **429**, 857 (2004).
[38]P. M. Biesheuvel, J. Phys.: Condens. Matter **16**, L499 (2004).
[39]J. W. Merrill, S. K. Sainis, and E. R. Dufresne, Phys. Rev. Lett. **103**, 138301 (2009).
[40]T. Vissers, A. Imhof, F. Carrique, A. V. Delgado, and A. van Blaaderen, J. Colloid Interface Sci. **361**, 443 (2011).
[41]D. El Masri, P. van Oostrum, F. Smallenburg, T. Vissers, A. Imhof, M. Dijkstra, and A. van Blaaderen, Soft Matter **7**, 3462 (2011).
[42]F. Smallenburg, N. Boon, M. Kater, M. Dijkstra, and R. van Roij, J. Chem. Phys. **134**, 074505 (2011).
[43]L. Berthier and W. Kob, J. Phys.: Condens. Matter **19**, 205130 (2007).
[44]E. Sanz and D. Marenduzzo, J. Chem. Phys. **132**, 194102 (2010).
[45]S. Jabbari-Farouji and E. Trizac, J. Chem. Phys. **137**, 054107 (2012).
[46]E. J. W. Verwey and J. Th. G. Overbeek, *Theory of the Stability of Lyophobic Colloids* (Elsevier, Amsterdam, 1948).
[47]P. J. Steinhardt, D. R. Nelson, and M. Ronchetti, Phys. Rev. B **28**, 784 (1983).
[48]W. Lechner and C. Dellago, J. Chem. Phys. **129**, 114707 (2008).
[49]P. R. ten Wolde, M. J. Ruiz-Montero, and D. Frenkel, Phys. Rev. Lett. **75**, 2714 (1995).
[50]M. Buzzacchi, P. Sollich, N. B. Wilding, and M. Müller, Phys. Rev. E **73**, 046110 (2006).
[51]R. M. L. Evans, D. J. Fairhurst, and W. C. K. Poon, Phys. Rev. Lett. **81**, 1326 (1998).